Chem Catalysis

CellPress
OPEN ACCESS

Article

# Building a photocatalyst library of MR-TADF compounds with tunable excited-state redox potentials

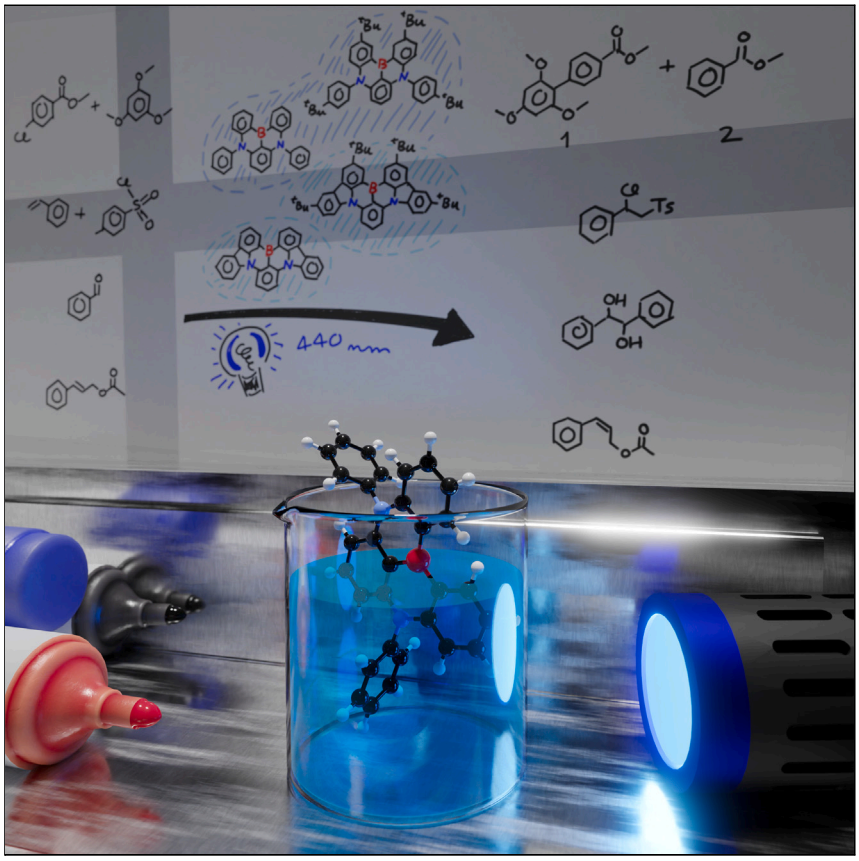


This study investigated B/N-doped MR-TADF materials as photocatalysts across a range of photoinduced electron and energy transfer reactions. These photocatalysts are strongly photoreducing, evidenced by their ability to photocatalyze the dehalogenation of electron-rich aryl halides. Their reactivity complements the MR-TADF photocatalyst **DiKTa**, which we previously reported.

Lea Hämmerling, Eli Zysman-Colman

eli.zysman-colman@st-andrews.ac.uk

## Highlights

Four MR-TADF compounds have been applied as photocatalysts in PET and PEnT reactions

They are strongly photoreducing and their optoelectronic properties are tunable

These four compounds could promote the photocatalyzed dehalogenation of aryl halides

***t*DABNA** shows high efficiency in an ATRA reaction, outperforming **4CzIPN**

Hämmerling & Zysman-Colman, Chem Catalysis 4, 101061
August 15, 2024 
Published by Elsevier Inc.
https://doi.org/10.1016/j.checat.2024.101061

Chem Catalysis

CellPress
OPEN ACCESS

Article

# Building a photocatalyst library of MR-TADF compounds with tunable excited-state redox potentials

Lea Hämmerling[1] and Eli Zysman-Colman[1,2,*]

## SUMMARY

**Epitomized by 4CzIPN, donor-acceptor (D-A) thermally activated delayed fluorescence (TADF) compounds based on the carbazoyl dicyanobenzene have now become widely used, as they are sustainable photocatalyst alternatives to organometallic complexes owing to their similar optoelectronic properties compared with many of the iridium-based photocatalysts. Multiresonant TADF (MR-TADF) compounds offer distinct advantages over D-A TADF compounds, as they have more intense low-energy absorption bands, offering faster reaction kinetics, and are less sensitive to the polarity of the environment, mitigating undesired energy loss that typically accompanies the charge transfer (CT) excited states of the photocatalysts. Here, we report the assessment of strongly photoreducing boron- and nitrogen-doped MR-TADF compounds DABNA-1, *t*DABNA, CzBN, and DtBuCzB across a range of benchmark photochemical reactions. The structural differences between the members of this library of photocatalysts enable modulation of their ground- and excited-state redox potentials. These photocatalysts performed competitively compared to the literature-known 4CzIPN, Ph-PTZ, and *fac*-Ir(ppy)$_3$.**

## INTRODUCTION

Photocatalysis has cemented itself as an important tool for synthetic organic chemists, allowing for thermally inaccessible transformations to be conducted at room temperature utilizing visible light energy as the driving force.[1–3] During a photocatalytic reaction, the photocatalyst (PC) is excited into an excited state (PC*) by absorbing incident visible light. After rapid internal conversion processes, the PC* can subsequently interact with substrates (Ss) in several different ways. If the PC* transfers its energy to S, the activation mode is termed photoinduced energy transfer (PEnT) and can occur via either a Dexter or a Förster energy transfer mechanism.[4] If the interaction involves single-electron transfer, the mechanism is termed photoinduced electron transfer (PET), occurring via oxidative quenching (where the PC* is initially oxidized to $PC^{+\bullet}$ and S is reduced to $S^{-\bullet}$) or reductive quenching (where the PC* is reduced to $PC^{-\bullet}$ and S is oxidized to $S^{+\bullet}$) catalytic cycles. Collectively, PET photocatalysis is commonly referred to as photoredox catalysis.

In homogeneous photocatalysis, broadly, PCs can be divided into two main families: transition metal complexes and organic PCs. The initial explosion of interest in photocatalytic reactions over the past 15 years or so has been accompanied by the frequent use of organometallic Ru(II) and Ir(III) complexes as PCs (Figure S2), which interact with Ss exclusively from their triplet excited state. Despite their ability to

## THE BIGGER PICTURE

Multiresonant thermally activated delayed fluorescence (MR-TADF) materials are used as emitters in high-performance organic light-emitting diodes (OLEDs). The photophysical properties of such emitters, including strongly absorptive absorption bands in the visible regime and minimal solvatochromism of the emissive excited state, suggest that these compounds should act as potent photocatalysts. Herein, Hämmerling and Zysman-Colman report the performance of four boron-containing MR-TADF compounds in initiating photoinduced electron transfer and photoinduced energy transfer reactions. The ground- and excited-state redox potential as well as the triplet energies could be tuned as a function of the choice of donor moieties embedded within the MR-TADF core. Mechanistic investigations revealed that these compounds act as precatalysts to initiate the photoredox reactions. Notably, DABNA-1 could quantitatively dehalogenate the model substrate methyl 4-chlorobenzoate.

photocatalyze a wide range of reactions, platinoid metals are scarce and costly, and the toxicity profile is suboptimal, particularly if late-stage photocatalysis is to be used in pharmaceutical synthesis.[5–7] Among the most prominent organic PCs are either natural organic dyes, like eosin Y,[8,9] rose bengal,[10,11] fluorescein,[5,12,13] and acridinium salts,[14,15] or donor-acceptor (D-A) thermally activated delayed fluorescence (TADF) emitters originally designed for use in organic light-emitting diodes (LEDs).[3,16]

Unlike fluorescent dyes, the singlet ($S_1$) and triplet ($T_1$) excited states of TADF compounds are both populated, facilitated by a small energy gap ($\Delta E_{ST}$) between the two that permits exciton cycling by a combination of intersystem crossing (ISC) and reverse intersystem crossing (RISC) (Figure 1). The small $\Delta E_{ST}$ results from the small exchange integral between the highest occupied molecular orbital (HOMO) and the lowest unoccupied molecular orbital (LUMO). In D-A TADF emitters, this separation is most commonly achieved when the donor and acceptor adopt a strongly twisted conformation such that electronic communication between the two is very weak. Luo and Zhang[17] first demonstrated that prototypical TADF carbazolyl dicyanobenzenes (CDCBs) like **4CzIPN** (see Figures 3D and S1A) can be highly efficient visible-light PCs. Due to its photophysical properties being remarkably similar to those of the widely used PC **[Ir(dF(CF$_3$)-ppy)$_2$(dtbbpy)]PF$_6$**, **4CzIPN** has been repeatedly shown to be a highly versatile and competitive PC across a broad range of transformations.[3] Modulating the structure of **4CzIPN** and its derivatives results in the facile tuning of their ground- and excited-state redox potentials, making this class of PCs much more versatile than the naturally occurring organic dyes historically used for photocatalysis.[17,18] Beyond **4CzIPN** and structurally related PCs, a small number of other D-A TADF compounds have been explored as PCs. Recently, we reported that **pDTCz-DPmS** (Figure S1B) was a versatile PC across a range of photocatalytic reactions.[19] Bouzrati-Zerelli et al. used a similar D-A PC containing electron-deficient diphenyl sulfone to initiate a free radical polymerization of methacrylates.[20] Hojo et al. showed that a group of imidazophenothiazine (**IPTZ**)-based TADF emitters (Figure S1C) can serve as efficient PCs in five different PEnT reactions.[21] This work was built upon related imidazoacridine-based TADF compounds that were demonstrated to photocatalyze [2 + 2] cycloadditions in a PEnT mechanism.[22]

We demonstrated that the multiresonant TADF (MR-TADF) emitters **DiKTa** ($E_{red}$* = 1.49 V and $E_{ox}$* = −1.16 V in MeCN[23]) and **Mes$_3$-DiKTa** ($E_{red}$* = 1.35 V and $E_{ox}$* = −1.04 V in MeCN[17]) are attractive compounds as PCs (Figure 2A), matching or even outperforming D-A TADF and organometallic PCs across a mechanistically broad range of reactions.[23] MR-TADF emitters are typically n- and p-doped nanographene compounds that have short-range charge transfer (SRCT) excited states that lead to relatively small $\Delta E_{ST}$.[24] Importantly, the SRCT state is less strongly influenced by the polarity of the solvent than long-range charge transfer (LRCT) states of D-A TADF compounds, meaning that less energy is lost in these compounds in polar solvents.[24] As well, due to their rigid structure, there is less geometric reorganization in the excited state, leading to bright, narrowband emission and intense low-energy absorption bands. The high molar absorptivity in the visible region of these bands is beneficial in photocatalysis, as it means that the concentration of PC* is higher and the rate of the reaction is generally faster.[3,25,26] In our previous study of **DiKTa** as a PC, we showed that the PC loading in a photo-Giese reaction could be lowered to 0.25 mol % from 1 mol % without a significant deleterious effect on the product yield.[23] By contrast, there was a significant drop in product yield at the lower PC loading when **4CzIPN** was used as the PC, which correlated with its lower molar

[1]Organic Semiconductor Centre, EaStCHEM School of Chemistry, University of St Andrews, St Andrews KY16 9ST, UK

[2]Lead contact

*Correspondence: eli.zysman-colman@st-andrews.ac.uk

https://doi.org/10.1016/j.checat.2024.101061

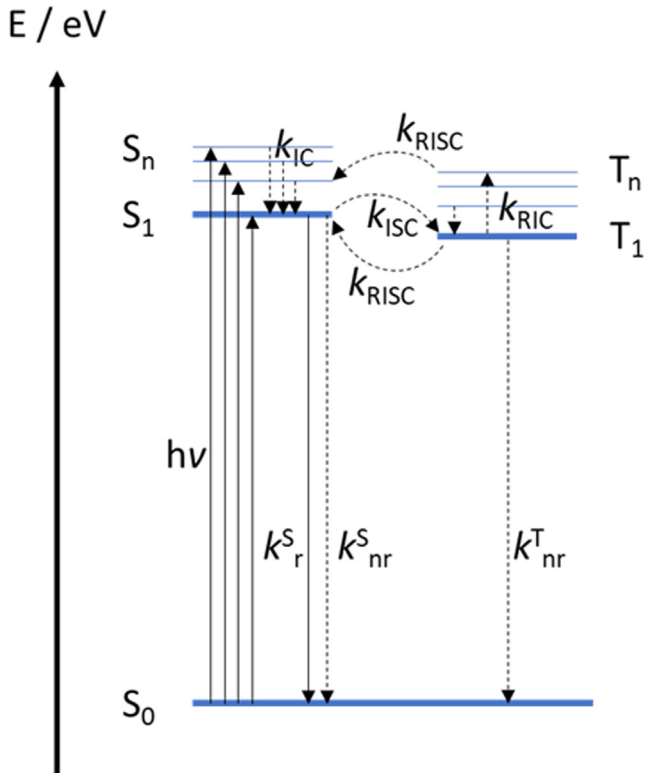


**Figure 1. Simplified Jablonski diagram showing relevant photophysical processes following photoexcitation in a TADF material**

$S_n$ and $T_n$ are higher-lying triplet states; hν describes the absorption of light, $k_{IC}$ the rate constant of internal conversion, $k_{ISC}$ the rate constant of intersystem crossing (ISC), $k_{RISC}$ the rate constant of reverse ISC, and $k_{RIC}$ the rate constant of reverse internal conversion. $k^S_{nr}$ and $k^T_{nr}$ are the rate constants of non-radiative decay from singlet and triplet states, respectively, and $k^S_r$ is the rate constant of radiative decay from the singlet state. $k^T_r$, not shown, is the rate constant of radiative decay from the triplet state and is taken as 0 $s^{-1}$.[55]

absorptivity at the photoexcitation wavelength; we also showed that the rate of product formation with **DiKTa** as the PC was much faster than with **4CzIPN** in an atom transfer radical addition (ATRA) reaction.[23]

From the literature, strongly photoreducing organic PCs include **Ph-PTZ** (**PTH**), **AZ1**, and **AZ2**, possessing excited-state oxidation potentials $E_{ox}$* of −2.10,[27] −2.34,[28] and −2.36 V,[28] respectively (Figures 3A–3C). Unfortunately, the low-energy absorption bands of each of these PCs have low molar absorptivity (**Ph-PTZ**, $\lambda_{abs}$ = 300 nm in MeCN, ε not quantified[29]; **AZ1** and **AZ2**, $\lambda_{abs}$ = 373 nm, ε = 5.2 × $10^3$ $M^{-1}cm^{-1}$ and $\lambda_{abs}$ = 370 nm, ε = 4.9 × $10^3$ $M^{-1}cm^{-1}$ in N,N-dimethylformamide [DMF]).[28] Therefore, a strongly photoreducing PC possessing an intense low-energy absorption band in the visible region would be highly desirable. Despite the significant promise of these MR-TADF molecules, **DiKTa** and **Mes$_3$DiKTa** are only moderately photoreducing ($E_{ox}$* = −1.16 and −1.05 V, respectively) yet are strong photooxidizing agents ($E_{red}$* = 1.49 and 1.31 V for **DiKTa** and **Mes$_3$DiKTA**) (Figure 2A). These two PCs therefore have behaved similar to **4CzIPN** ($E_{ox}$* = −1.04 and $E_{red}$* = 1.35 V[17]) and thus would not be appropriate to use in reactions that require more highly photoreducing catalysts. We thus aimed to identify MR-TADF compounds that would be more strongly photoreducing and still leverage the distinct advantages of the photophysical properties endemic to this class of compounds.

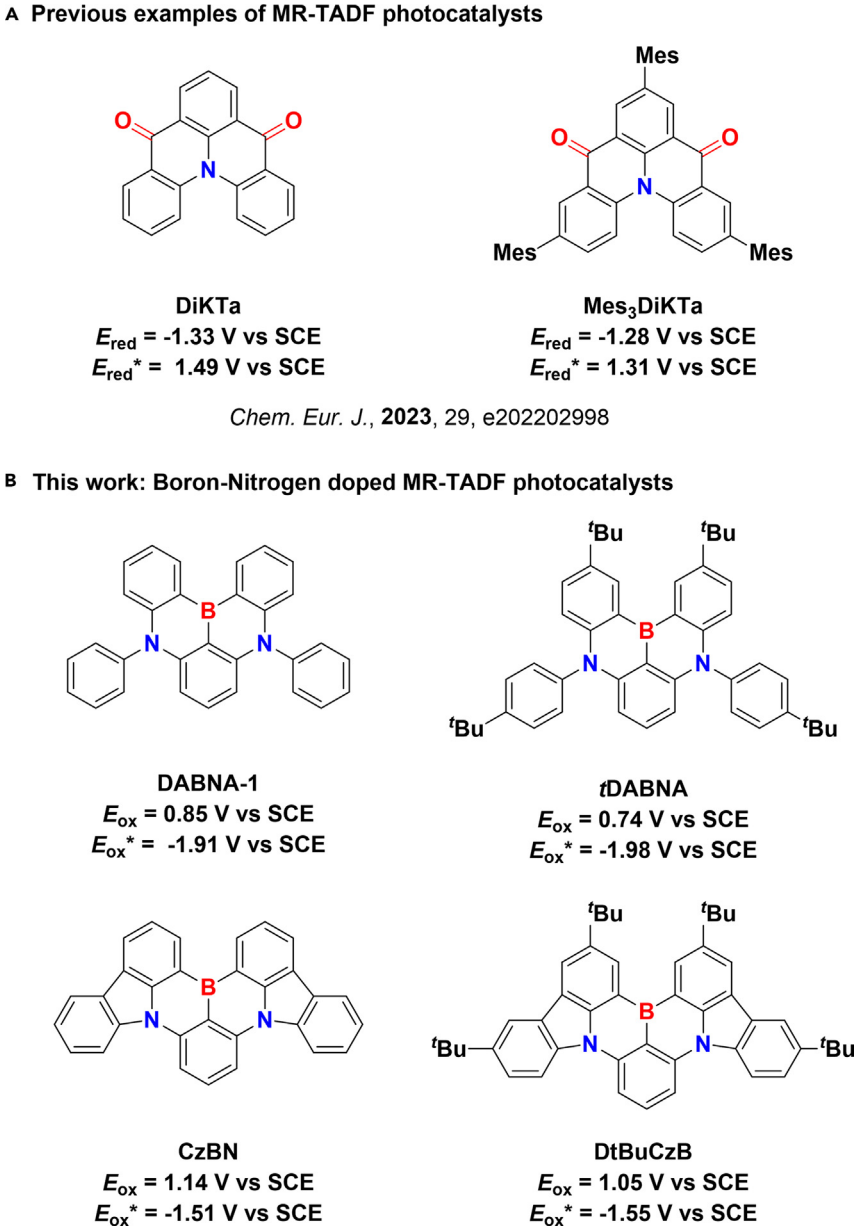


**Figure 2. Structures of multiresonant thermally activated delayed fluorescence (MR-TADF) photocatalysts (PCs)**

(A) Previous examples **DiKTa** and **Mes3DiKTa** (values measured in MeCN).

(B) Boron-nitrogen-based MR-TADF compounds explored as PCs in this work (values measured in DCM).

Here, we investigated four boron/nitrogen MR-TADF emitters as PCs. These include **DABNA-1**, first reported by Hatakeyama et al. (Figure 2B),[30] which has an intense absorption band in dichloromethane (DCM) at $\lambda_{abs}$ of 437 nm ($\varepsilon$ = 24.6 × $10^3$ $M^{-1}$ $cm^{-1}$)[30]; a *tert*-butyl-substituted derivative, ***t*DABNA**, that has a slightly red-shifted, intense absorption band at $\lambda_{abs}$ of 445 nm[31]; a carbazole analog to **DABNA-1**, **CzBN**, that has a red-shifted absorption band at $\lambda_{abs}$ of 458 nm in DCM[32]; and a *tert*-butyl-substituted analog, **DtBuCzB**, that possesses the most red-shifted absorption band of the four compounds at $\lambda_{abs}$ of 467 nm in

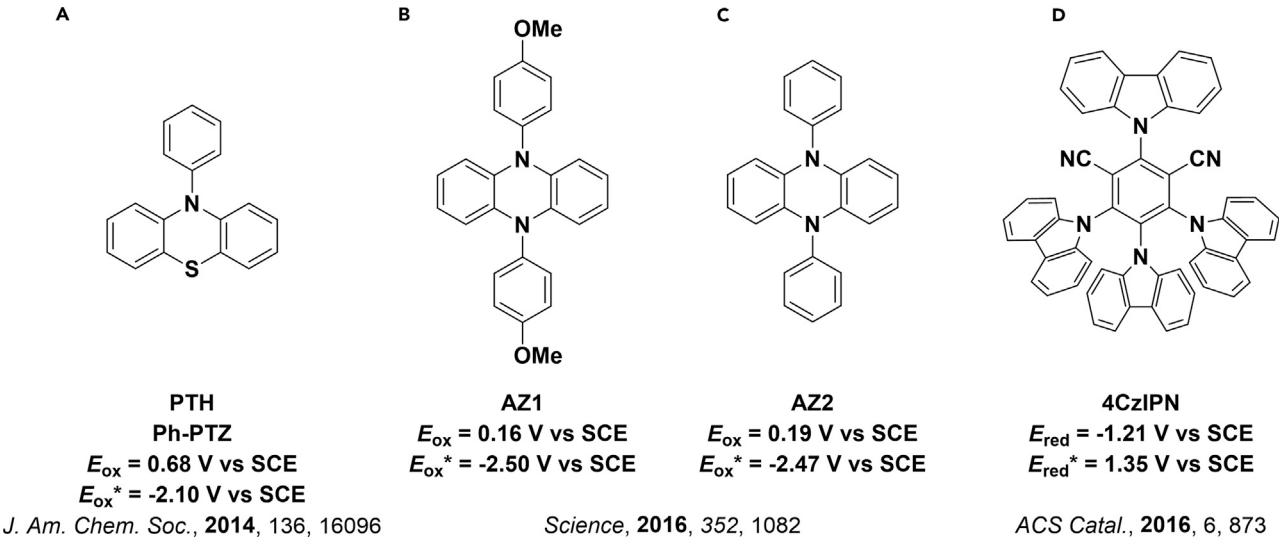


**Figure 3. Organic literature photocatalysts mentioned in the text**

Chemical structures of strongly photoreducing photocatalysts (A) **Ph-PTZ**, phenazine derivatives (B) **AZ1** and (C) **AZ2**, and (D) **4CzIPN** and the tatracarbazolyl isophthalonitrile compound.

toluene (PhMe).[33] For ***t*DABNA**, **CzBN**, and **DtBuCzB**, no molar absorptivity data were reported. The four PCs are mildly to strongly photoreducing, ranging from **CzBN** ($E_{ox}$* = −1.51 eV) to ***t*DABNA** ($E_{ox}$* = −1.98 eV), the latter of which is of comparable strength to two strongly photoreducing literature PCs, ***fac*-Ir(ppy)$_3$** ($E_{ox}$* = −1.73 V)[34] and **Ph-PTZ** ($E_{ox}$* = −2.10 V)[27] (Figure 4).

## RESULTS AND DISCUSSION

### Synthesis and photophysical investigations

The structures were synthesized following literature procedures (Figures S4–S24), and the photophysical and electrochemical properties of **DABNA-1**, ***t*DABNA**, **CzBN**, and **DtBuCzB** were investigated in PhMe, tetrahydrofuran (THF), dichloromethane (DCM), MeCN, and DMF, commonly used solvents for photocatalysis reactions, and their properties were cross-compared to those of the archetypal TADF PC **4CzIPN**. Cyclic voltammetry (CV) and differential pulse voltammetry (DPV) scans of **DABNA-1** are shown in Figure S25A. In MeCN and DMF, the reduction was found to be irreversible at $E_{red}$ of −2.24 and −2.14 V vs. saturated calomel electrode (SCE), respectively, values that are comparable to the literature PC ***fac*-Ir(ppy)$_3$** ($E_{red}$ of −2.19 V vs. SCE in MeCN[35]); no reduction was observed in THF or DCM, as the electron affinity lies beyond the solvent window. The oxidation of **DABNA-1** is irreversible in THF, MeCN, and DMF but reversible in DCM. The $E_{ox}$ values are broadly similar in DMF, MeCN, and DCM at $E_{ox}$ of 0.86, 0.80, and 0.85 V vs. SCE, respectively; however, this changes significantly in THF ($E_{ox}$ of 1.01 V), possibly due to the formation of a THF adduct upon oxidation. The oxidation potentials are more positively shifted than of that of ***fac*-Ir(ppy)$_3$** ($E_{ox}$ of 0.77 V vs. SCE in MeCN[35]). Due to the reduced solubility of ***t*DABNA**, the CV and DPV could only be recorded in THF, DCM, and DMF (Figure S25B). None of these three solvents has a redox window sufficiently broad that permitted the recording of the reduction of this compound, suggesting that its reduction is even more negative than that of **DABNA-1**. The $E_{ox}$ of ***t*DABNA** is cathodically shifted compared to **DABNA-1**, having values of 0.84, 0.74, and 0.91 V vs. SCE in DMF, DCM, and THF, respectively; notably, as with **DABNA-1**, the $E_{ox}$ of ***t*DABNA** is the most anodically shifted in

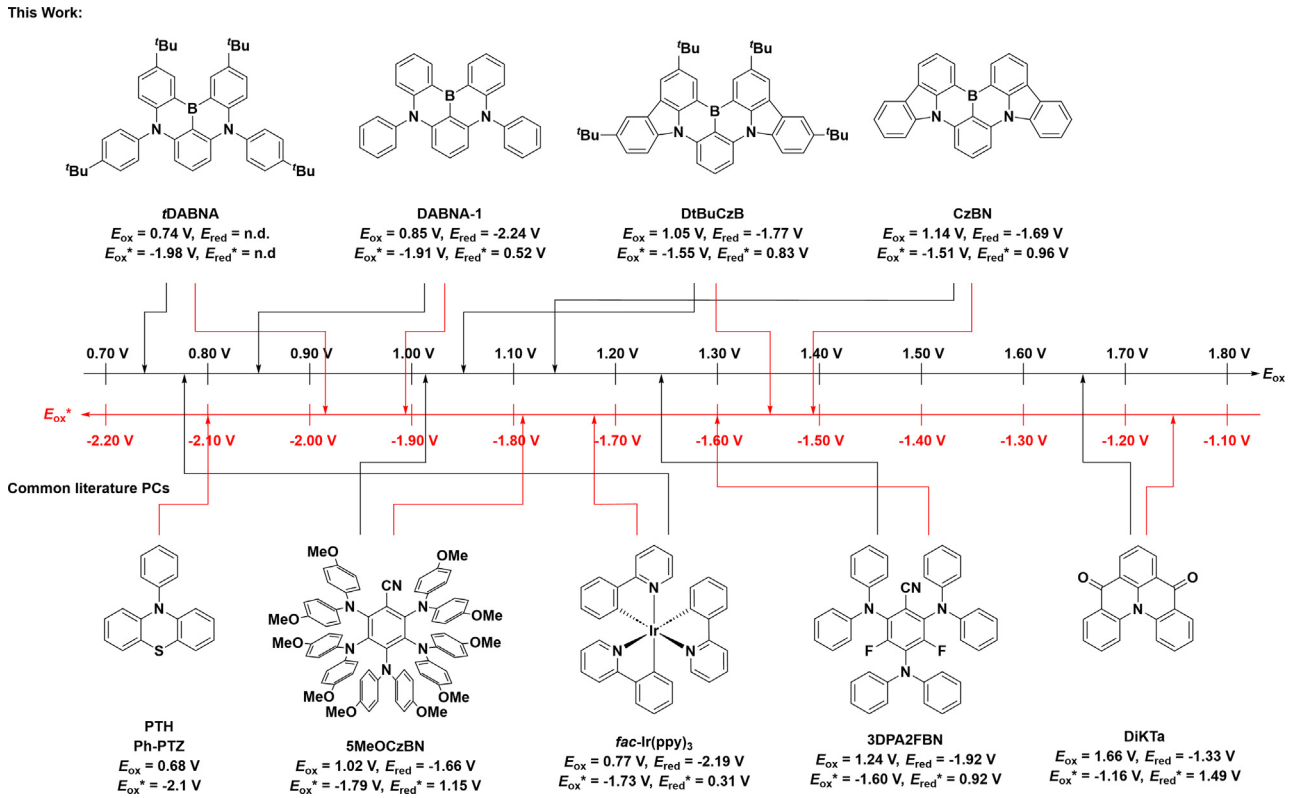


**Figure 4. Redox potentials of the four investigated materials compared to those of selected literature photocatalysts**

Structures and redox potentials of the MR-TADF emitters investigated as photocatalysts in this work and a comparison to photocatalysts known from the literature (redox potentials of **Ph-PTZ** taken from Treat et al.[56] in MeCN, **3DPA2FBN** and **5MeOCzBN** taken from Speckmeier et al.[18] in MeCN, and *fac*-Ir(ppy)$_3$ from Koike and Akita[34] and Flamigni et al.[35] in MeCN).

THF. **CzBN** is only soluble in DCM (Figure S25C); compared to **DABNA-1** and ***t*DABNA**, its $E_{ox}$ is more positive, at 1.14 V, and the oxidation is reversible, but **CzBN** is not as oxidizing as **4CzIPN**, **DiKTa**, or [Ir(ppy)$_2$(dtbbpy)](PF$_6$)$_2$ ($E_{ox}$ of 1.52,[17] 1.66,[36] and 1.21 V[37] vs. SCE, respectively, in MeCN). The reduction of **CzBN** is likewise anodically shifted and irreversible at $E_{red}$ of −1.69 V (Figure S25C) compared to those of **DABNA-1** ($E_{red}$ = −2.24 V vs. SCE in MeCN) and ***t*DABNA** (no reduction peak observed in any solvent). For comparison, **CzBN** is more reducing than [Ir(ppy)$_2$(dtbbpy)](PF$_6$)$_2$ ($E_{red}$ of −1.51 V vs. SCE in MeCN[37]). The *tert*-butyl groups in **DtBuCzB** improved the solubility of this compound, and electrochemistry could be recorded in both THF and DCM. The oxidation wave is reversible at $E_{ox}$ of 1.21 and 1.05 V, respectively, similar in value to that of **CzBN** in DCM, while the reduction is irreversible at $E_{red}$ of −1.77 V in DCM (the electrochemical window of THF is not sufficiently broad for the reduction to be recorded in this solvent) (Figure S25D). The collated electrochemical data are found in Tables 1 and S1.

The absorption profiles of **DABNA-1**, **tDABNA**, **CzBN**, and **DtBuCzB** in THF are all similar, but the *tert*-butyl-substituted analogs have a more intense and red-shifted low-energy SRCT band, and the SRCT band of the carbazole analogs is red-shifted compared to the diphenylamine (DPA)-based compounds due to an enhanced conjugation in the former (Figure 5C; Table 1; Figure S26; Table S2). Importantly, each of these compounds has a low-energy absorption band that is significantly more intense than commonly used iridium PCs. For example, the ε for SRCT bands in THF of **CzBN** ($\lambda_{abs}$ = 457 nm), ***t*DABNA** ($\lambda_{abs}$ = 443 nm), and **DABNA-1** ($\lambda_{abs}$ =

**Table 1. Selected optoelectronic properties of DABNA-1, tDABNA, CzBN, and DtBuCzB and the literature-known photocatalysts 4CzIPN, fac-Ir(ppy)$_3$, DiKTa, and Ph-PTZ**

| Compound | $\lambda_{abs}$ (nm) | $\lambda_{PL}$ (nm) | $E_{0,0}$ (eV) | $E_{ox}$ (V) | $E_{red}$ (V) | $E_{ox}$* (V) | $E_{red}$* (V) | $E_{T1}$ (eV) |
|---|---|---|---|---|---|---|---|---|
| DABNA-1 | 438 | 461 | 2.76 | 0.85 | −2.24[a] | −1.91 | 0.52[a] | 2.65 |
| *t*DABNA | 444 | 466 | 2.72 | 0.74 | – | −1.98 | – | 2.64 |
| CzBN | 457 | 480 | 2.65 | 1.14 | −1.69 | −1.51 | 0.96 | 2.58 |
| DtBuCzB | 467 | 488 | 2.60 | 1.05 | −1.77 | −1.55 | 0.83 | 2.52 |
| 4CzIPN | 376 | 544 | 2.60 | 1.52[b] | −1.21[b] | −1.04[b] | 1.35[b] | 2.56[b] |
| *fac*-Ir(ppy)$_3$[c] | 375 | 494[d] | 2.53[e] | 0.77 | −2.19 | −1.73 | 0.31 | 2.50 |
| [Ir(ppy)2(dtbbpy)]PF$_6$[f] | 415s | 591 | 2.17 | 1.21 | −1.51 | −0.96 | 0.66 | 2.52 |
| [Ru(bpy)$_3$](PF$_6$)$_2$[g] | 452 | 615 | 2.10 | 1.29 | −1.33 | −0.81 | 0.77 | 2.12[h] |
| DiKTa[i] | 436 | 467 | 2.82 | 1.66 | −1.33 | −1.16 | 1.49 | 2.62[j] |
| Ph-PTZ[k] | <300 | 445 | 2.78 | 0.68 | – | −2.10 | – | – |

Values are reported in dichloromethane unless otherwise noted. $\lambda_{abs}$ is the lowest energy absorption band. $E_{0,0}$ is determined by the intersection between normalized absorption and emission spectra (Figures S30–S34). Redox potentials are given vs. SCE and are obtained from the maxima in the DPV of the reduction and oxidation peaks. Excited-state redox potentials were calculated from $E_{ox}^* = E_{ox} - E_{0,0}$ and $E_{red}^* = E_{red} + E_{0,0}$. $E_{S1}$ and $E_{T1}$ were determined by the onsets of the steady-state and delayed emission spectra (measured 1 ms after excitation with gate time of 9 ms), respectively, measured in 2-MeTHF glass at 77 K.

[a]Measured in MeCN.

[b]Taken from Luo and Zhang[17] in MeCN.

[c]Taken from Koike and Akita[34] and Flamigni et al.[35]

[d]Measured in alcoholic glass.

[e]In 2-MeTHF from Sajoto et al.[57]

[f]Taken from Lowry et al.,[37] Chen et al.,[58] and Ladouceur et al.[59] in MeCN.

[g]Taken from Juris et al.[60,62] and Kalyanasundaram.[61] in MeCN.

[h]Measured in aqueous solution.

[i]Taken from Hall et al.[36] in MeCN.

[j]Measured in toluene.

[k]Taken from Discekici et al.[29] and Treat et al.[56] in MeCN.

439 nm) are 48.1 × 10$^3$, 15.2 × 10$^3$, and 26.3 × 10$^3$ M$^{-1}$ cm$^{-1}$, which are at least four times more intense than that of ***fac*-Ir(ppy)$_3$** ($\varepsilon$ = 7.2 × 10$^3$ M$^{-1}$ cm$^{-1}$ at $\lambda_{abs}$ = 375 nm[35] in MeCN) or **[Ir(ppy)$_2$(dtbbpy)](PF$_6$)** ($\varepsilon$ = 3.4 × 10$^3$ M$^{-1}$ cm$^{-1}$ at $\lambda_{abs}$ = 422 nm in THF; Figure S55). Notably, these bands are also more absorptive than the LRCT band of **4CzIPN** ($\varepsilon$ = 15 × 10$^3$ M$^{-1}$ cm$^{-1}$ at $\lambda_{abs}$ = 369 nm in THF) (Figure S28A). Crucially, the molar absorptivity of the MR-TADF compounds in the blue region of the visible light spectrum is significantly higher compared to the other strongly photoreducing PCs highlighted in Figure S3 ($\varepsilon$ = 24 × 10$^3$, 14 × 10$^3$, 21 × 10$^3$, and 15 × 10$^3$ M$^{-1}$ cm$^{-1}$ for **DABNA-1**, ***t*DABNA**, **CzBN**, and **DtBuCzB**, respectively, in THF at 440 nm, while **Ph-PTZ** does not absorb at 440 nm).[29]

In THF, **DABNA-1**, **tDABNA**, **CzBN**, and **DtBuCzB** emit at $\lambda_{PL}$(photoluminescence peak maxima) of 453, 458, 475, and 483 nm (Figure 5B), emissions that are blue-shifted compared to that of **4CzIPN** at $\lambda_{PL}$ = 528 nm (Figure S28B). Acquisition of the emission profiles in different solvents confirmed the small degree of positive solvatochromism (Figures S27 and S29; Table S3). This implies that the singlet optical gap $E_{0,0}$ for all four compounds remains broadly the same across the four solvents (Figures S30–S34). The largest variance in $E_{0,0}$ was observed for ***t*DABNA** at 0.04 eV (Table S4). In contrast, the emission of **4CzIPN** undergoes more significant stabilization in polar media, reflected in the wider range of $E_{0,0}$ values spanning a difference of 0.10 eV. Owing in part to their large optical gaps, all four catalysts are strongly photoreducing, with $E_{ox}^*$ = −1.91, −1.98, −1.51, and −1.55 for **DABNA-1**, ***t*DABNA**, **CzBN**, and **DtBuCzB**, respectively, in DCM. These values are much more negative than those of **4CzIPN** ($E_{ox}^*$ = −1.04 V) and **DiKTa** ($E_{ox}^*$ = −1.16 V) and comparable to those of ***fac*-Ir(ppy)$_3$** ($E_{ox}^*$ = −1.73 V in MeCN)[34] and **Ph-PTZ** ($E_{ox}^*$ = −2.10 V in MeCN).[27]

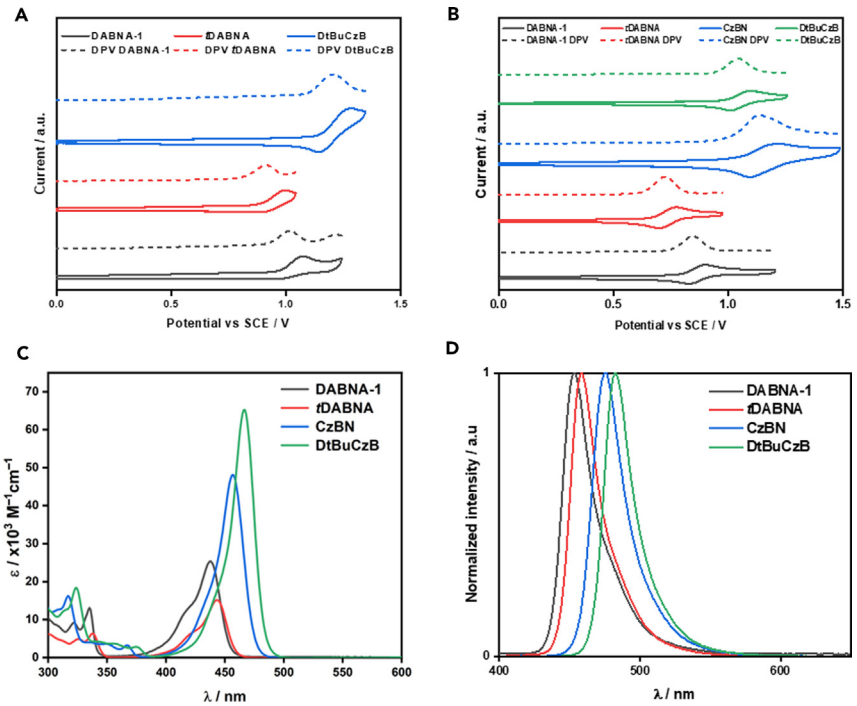


**Figure 5. Electrochemical and photophysical properties of DABNA-1, tDABNA, CzBN, and DtBuCzB**

(A and B) CVs and DPVs of **DABNA-1**, **tDABNA**, **CzBN**, and **DtBuCzB** in (A) DCM (note that the CV and DPV of **CzBN** could not be measured in this solvent), scan rate 0.1 V/s, and (B) THF, scan rate 0.1 V/s.

(C) UV-vis absorption spectra of **DABNA-1**, **tDABNA**, **CzBN**, and **DtBuCzB** in THF.

(D) Normalized steady-state PL spectra for **DABNA-1** ($\lambda_{exc}$ = 340 nm), **tDABNA** ($\lambda_{exc}$ = 390 nm), **CzBN** ($\lambda_{exc}$ = 400 nm), and **DtBuCzB** ($\lambda_{exc}$ = 425 nm) in THF. Measurements were performed under air and at room temperature.

The singlet and triplet excited-state energies were measured in 2-MeTHF glass at 77 K (Figure S35 and Table S5). The $S_1$ energy was inferred from the onset of the steady-state emission, while the $T_1$ energy was determined from the time-gated emission (acquisition 1–9 ms after excitation). **DABNA-1** has the highest excited-state energies of the four compounds ($S_1$ = 2.81 eV, $T_1$ = 2.65 eV), while **DtBuCzB** has the lowest energies ($S_1$ = 2.66 eV, $T_1$ = 2.52 eV). Their excited-state energies are comparable to those of **DiKTa** ($S_1$ = 2.82 eV, $T_1$ = 2.62 eV in PhMe) and ***fac*-Ir(ppy)$_3$** ($T_1$ = 2.50 eV in MeCN).[35]

We next assessed the photostability of the four compounds in each of the solvents by comparing their absorption spectra before and after photoexcitation using a 440 nm LED (Figure S37). We have previously assessed the photostability of a number of well-known PCs using a slightly different photoreactor setup, in a range of photocatalyzed energy and electron transfer reaction conditions,[38] where we observed poor photostability across the family of organic and organometallic PCs; indeed, other studies have shown as well that many PCs are not photostable under photoredox catalysis conditions such as these.[38–41] To better understand the degree of photostability of these four MR-TADF compounds in different solvents, we cross-compared their behavior with the widely used organic PC **eosin Y** using the same photoreactor setup (Figures S36 and S38).

In MeCN, the absorption spectra of all four MR-TADF emitters and **eosin Y** remained broadly unchanged upon photoirradiation for 24 h. In THF, the

diphenylamine-based emitters **DABNA-1** and ***t*DABNA** were found to be photostable, showing no obvious changes in the absorption spectra (Figure S37A and S37B); however, the SRCT band in the absorption spectra of **CzBN** and **DtBuCzB** after irradiation is significantly blue-shifted (Figures S36C and S36D). In THF, **eosin Y** is not photostable, reflected in changes in the absorption spectrum upon irradiation (Figure S37E). Curiously, in DCM the photostability behavior of the four MR-TADF emitters is the opposite of that observed in THF, where there is no appreciable change in the absorption spectra of **CzBN** and **DtBuCzB**, while the SRCT band in **DABNA-1** and ***t*DABNA** is red-shifted, indicating photodecomposition. In DCM, **eosin Y** is likewise not photostable, again, evidenced by changes in the absorption spectrum upon irradiation. Considering the structural differences between **DABNA-1** and ***t*DABNA** compared to **CzBN** and **DtBuCzB**, it is evident that the inclusion of diphenylamine groups leads to an increased photostability in THF, while the structures with carbazole are more photostable in DCM.

## Photocatalysis

### *Oxidative quenching photoredox catalysis*

Given the strong photoreducing power of all four PCs, we explored their use in the challenging dehalogenation reaction of aromatic halides. Methyl 4-chlorobenzoate has a reduction potential of $E_{red} = -2.0$ V measured in MeCN (Figure S46A). **Ph-PTZ** has been reported to photoreduce this S to methyl benzoate in 100% yield in MeCN.[27] The reaction conditions include the use of an amine as a sacrificial reductant to regenerate PC from $PC^{\bullet+}$ following oxidative quenching with methyl 4-chlorobenzoate.[27] Using these conditions, Bryden et al. showed that the TADF compound DMAC-TRZ derivatives act as effective precatalysts in the photodehalogenation of Ss as challenging as 3-bromoanisole ($E_{red} = -2.59$ V vs. SCE).[42] However, to mechanistically exclude halogen-atom transfer (XAT), where the radical cation of the sacrificial amine extracts the halogen atom from the S,[43] we adjusted the reaction conditions to intercept the aryl radical with 1,3,5-trimethoxybenzene (TMB) to target compound **1** (Table 2) as the main product (Figures S39–S45).

Both **Ph-PTZ** and **DABNA-1** (Table 2, entries 2 and 5) can promote the quantitative dehalogenation of methyl 4-chlorobenzoate; however, coupling with the radical trap is not efficient and results in a roughly 50:50 mixture of dehalogenated product to coupled product for **Ph-PTZ** as well as **DABNA-1**. In MeCN-$d_3$, only the coupled product was observed in both the $^1$H NMR spectrum and the gas chromatography-mass spectrometry (GC-MS), implying that the proton needed for the dehalogenated product (**2**) is abstracted from the solvent (Figure S45). Using pivalonitrile instead of acetonitrile as the solvent led to a slight improvement in the ratio of coupled product to dehalogenated product (Table 2, entry 6); however, this was accompanied by an overall drop in yield.

Both **Ph-PTZ** and **DABNA-1** act as equally good PCs for this reaction; however, lower energy excitation can be used with **DABNA-1** (Table 2, entry 5), while at 440 nm a trace product is formed using **Ph-PTZ** (Table 2, contrast entries 2 and 3). This is important, as certain organic compounds absorb at 390 nm but not at 440 nm. For example, the use of methyl 4-iodobenzoate yielded 21% of **1** and 19% of **2** in the absence of a PC when irradiated at 390 nm, but no reaction was observed when the S was irradiated at 440 nm (Table S6). When using **DABNA-1** as a PC in the reaction with methyl 4-iodobenzoate, products **1** and **2** were formed in yields of 24% and 27%, respectively (Table S6). When **Ph-PTZ** is used as the PC ($\lambda_{exc} = 390$ nm), yields of 33% and 40% for **1** and **2**, respectively, were obtained, largely mirroring the efficiency of the background reaction (Table S6). Upon irradiation at 440 nm, none of

**Table 2. Dehalogenatative cross-coupling reactions between methyl 4-chlorobenzoate (MCB) and 1,3,5-trimethoxybenzene (TMB)**

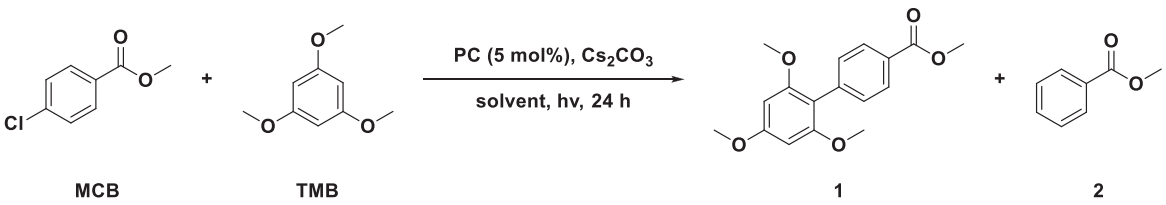


MCB TMB 1 2

| Entry | Photocatalyst | Condition | Yield 1 (%) | Yield 2(%) |
|---|---|---|---|---|
| 1 | None | $\lambda_{exc}$ = 440 nm, MeCN | 0 ± 0 | 0 ± 0 |
| 2 | Ph-PTZ | $\lambda_{exc}$ = 390 nm, MeCN | 47 ± 5 | 49 ± 2 (quant.[a]) |
| 3 | Ph-PTZ | $\lambda_{exc}$ = 440 nm, MeCN | trace | trace |
| 4 | Ph-PTZ | $\lambda_{exc}$ = 390 nm, MeCN, 10 equiv. TMB | 65 ± 1 | 34 ± 5 |
| 5 | DABNA-1 | $\lambda_{exc}$ = 440 nm, MeCN | 47 ± 4 | 48 ± 2 |
| 6 | DABNA-1 | $\lambda_{exc}$ = 440 nm, pivalonitrile | 34 ± 1 | 19 ± 1 |
| 7 | 4CzIPN | $\lambda_{exc}$ = 440 nm, MeCN | 0 ± 0 | 0 ± 0 |
| 8 | *fac*-Ir(ppy)$_3$ | $\lambda_{exc}$ = 440 nm, MeCN | trace | trace |
| 9 | [Ru(bpy)$_3$](PF$_6$)$_2$ | $\lambda_{exc}$ = 440 nm, MeCN | 0 ± 0 | 0 ± 0 |
| 10 | DABNA-1 | $\lambda_{exc}$ = 440 nm, THF | 0 ± 0 | 18 ± 1 |
| 11 | *t*DABNA | $\lambda_{exc}$ = 440 nm, THF | 0 ± 0 | 17 ± 0 |
| 12 | CzBN | $\lambda_{exc}$ = 440 nm, THF | 0 ± 0 | 26 ± 2 |
| 13 | DtBuCzB | $\lambda_{exc}$ = 440 nm, THF | 0 ± 0 | 21 ± 0 |

MCB (0.1 mmol), TMB (0.5 mmol), $Cs_2CO_3$ (0.2 mmol), and PC (5 mol %) in 1 mL solvent under a nitrogen atmosphere. Irradiated for 24 h at room temperature. Yield determined by $^1$H NMR spectroscopy using 1,3-dinitrobenzene or dibromomethane as an internal standard, averaged over two experiments.
[a]Literature-reported yield after 24 h in MeCN using $NBu_3$ and $HCO_2H$ as an additive and $\lambda_{exc}$ = 380 nm[27].

**4CzIPN** ($E_{ox}$* = −1.04 V),[17] **[Ru(bpy)$_3$](PF$_6$)$_2$** ($E_{ox}$* = −0.81 V),[44] or ***fac*-Ir(ppy)$_3$** ($E_{ox}$* = −1.73 V)[34] could photocatalyze the reaction (Table 2, entries 7–9), owing to their insufficient photoreducing power to reduce methyl 4-chlorobenzoate ($E_{red}$ = −2.0 V).

Surprisingly, Stern-Volmer quenching studies revealed that there is no quenching of the emission of **DABNA-1** with either the aryl halide or TMB (Figures S46D and S46E). We thus investigated whether there is the formation of an electron donor-acceptor (EDA) complex by UV-visible (UV-vis) absorption spectroscopy between the electron-rich TMB and the aryl halide for all three aryl halides (Figure S46B). The absorption spectra revealed no emergence of a low-energy band, and thus, we concluded that there is no evidence for the formation of EDA complexes in these solutions. We then studied the photostability of **DABNA-1** under the reaction conditions by comparing the absorption of the reaction mixture prior to and after photoexcitation. The absorption spectrum of the reaction mixture is the same as that of **DABNA-1** in MeCN prior to irradiation, but it changes significantly post-reaction, pointing to a photoinstability of the PC under the reaction conditions (Figure S46C). Thus, **DABNA-1** for this reaction acts as a pre-PC. We then studied the photodegradation of the PC and the formation of **1** and **2** as a function of time by $^1$H NMR and absorption spectroscopy (Figure 6). After 30 min, the intensity of the SRCT absorption band of **DABNA-1** decreased in intensity to 84% of its original, while the dehalogenated product was detected only in trace amounts. The intensity of this band decreased steadily to 27% of its original intensity at 5 h, while the yield of the dehalogenated product plateaued at 35%; however, after 24 h there was complete dehalogenation of methyl 4-chlorobenzoate.

We then proceeded to assess **CzBN**, ***t*DABNA**, and **DtBuCzB** as PCs in the same reaction, and due to their poor solubility in MeCN (and most other organic solvents), the

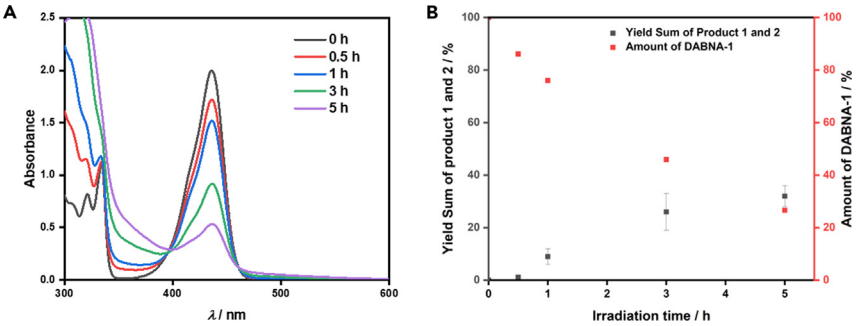


**Figure 6. Time-dependent study of the degradation of DABNA-1 and the formation of dehalogenated product in the dehalogenation reaction outlined in Table 2**

Reaction conditions were MCB (0.1 mmol), TMB (0.5 mmol), $Cs_2CO_3$ (0.2 mmol), and PC (5 mol %) in 1 mL MeCN under inert conditions, irradiated at 440 nm. Twelve reactions were run in parallel, of which three were analyzed after the given time had elapsed, one for absorption measurement (A) and two for determining the average yield and error (B) by $^1$H NMR spectroscopy in $CDCl_3$ using $CH_2Br_2$ as an internal standard. The percentage yield represents the combined yield of **1** and **2**. For the absorption measurements, after each time interval, 20 μL of the reaction mixture was taken and diluted further with 1 mL of MeCN before absorption measurements.

subsequent studies were conducted in THF. Unfortunately, this solvent was problematic for this reaction as there was no evidence of **1** with these PCs nor with **DABNA-1**, while **2** was formed in yields of 18%, 17%, 26%, and 21%, respectively, using **DABNA-1**, ***t*DABNA**, **CzBN**, and **DtBuCzB**. This outcome likely is due to the more easily abstractable proton from THF than from MeCN, leading to a much faster rate of hydrogen atom transfer (HAT) from the solvent to the aryl radical than trapping with TMB. Of the four PCs, **CzBN** produced the highest yield of dehalogenated product.

We also assessed the performance of these PCs in the photocatalytic ATRA reaction of styrene and *p*-toluenesulfonyl chloride (TsCl) (Figures S48–S50).[45,46] The generally accepted mechanism involves an oxidative quenching of the PC* by TsCl, generating a tosyl radical (Ts$^\bullet$), which engages in a radical addition onto the olefin. The benzylic radical is oxidized by PC$^{\bullet+}$, regenerating the ground-state neutral catalyst and forming a cationic intermediate that is subsequently trapped by the liberated chloride anion, or the benzylic radical abstracts a chloride atom from TsCl to form the final product, liberating Ts$^\bullet$ (Figure S47).[47] The reduction potential of TsCl ($E_{red}$ = −0.94 V vs. SCE)[46] is comfortably less negative than the $E_{ox}$* of these PCs (Table 1), meaning that all four PCs are capable of reducing TsCl. Separately, the PC$^{\bullet+}$ must be capable of oxidizing the carbon-centered radical following addition to the olefin; therefore, a moderate ground-state oxidation potential is also needed to turn over this reaction. D-A TADF emitters have been previously employed as effective PCs in atom transfer radical polymerization (ATRP) reactions, leading to polymers with narrow dispersity.[48,49] We previously studied the performance of different D-A TADF PCs in the ATRA reactions of TsCl and styrene; however, neither **4CzIPN** nor **pDTCz-DPmS** performed well with these two Ss, yielding, respectively, only 10% and 16% of the desired product.[19] The use of **[Ru(bpy)$_3$](PF$_6$)$_2$** ($E_{ox}$* = −0.86 V vs. SCE) as the PC has been shown to yield the product at 80% in MeCN[46] and 64% in DCM.[19] The MR-TADF library in this study was tested in this reaction as the PC in different solvents, with either one or two equivalents of styrene (Tables 3 and S8).

In general, the reaction is sluggish in THF, with the highest yield of 26% being obtained using ***t*DABNA** (Table 3, entry 4). A small solvent screen showed that in

**Table 3. Atom radical transfer reaction between styrene and tosyl chloride (TsCl)**

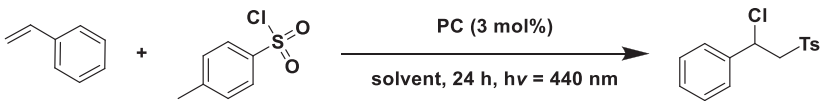


| Entry | Photocatalyst | Solvent | $^1$H NMR yield (%) |
|---|---|---|---|
| 1 | no catalyst | DCM | 0 ± 0 |
| 2 | DABNA-1 | THF | 23 ± 1 |
| 3 | DABNA-1 | MeCN | 10 ± 1 |
| 4 | DABNA-1 | DCM | 56 ± 0 |
| 5 | *t*DABNA | THF | 26 ± 2 |
| 6 | *t*DABNA | MeCN | 7 ± 2 |
| 7 | *t*DABNA | DCM | 63 ± 4 |
| 8 | CzBN | THF | 22 ± 9 |
| 9 | CzBN | MeCN | 13 ± 0 |
| 10 | CzBN | DCM | 42 ± 3 |
| 11 | DtBuCzB | THF | 17 ± 3 |
| 12 | DtBuCzB | MeCN | 11 ± 4 |
| 13 | DtBuCzB | DCM | 48 ± 5 |
| 14 | 4CzIPN | DCM | 39 ± 4 (10, 1 mol % PC loading[a]) |
| 15 | *fac*-Ir(ppy)$_3$ | DCM | 84 ± 2 (45, 1 mol % PC loading[b]) |
| 16 | [Ru(bpy)$_3$](PF$_6$)$_2$ | DCM | 89 ± 3 (80, 1 mol % PC loading[b]) |
| 17 | [Ir(ppy)$_2$(dtbbpy)](PF$_6$) | DCM | 71 ± 2 |

TsCl (0.25 mmol), styrene (0.50 mmol), and PC (3 mol %) in 1 mL solvent. Irradiated at 440 nm for 24 h at room temperature under a nitrogen atmosphere. Yield determined by $^1$H NMR spectroscopy using TMB as an internal standard.

[a]Literature-reported yield for **4CzIPN** in DCM after 24 h with $\lambda_{exc}$ = 390 nm with 1 mol % PC loading.[19]

[b]Literature-reported yield for ***fac*-Ir(ppy)$_3$** and **[Ru(bpy)$_3$]Cl$_2$** in MeCN after 24 h with $\lambda_{exc}$ = 455 nm with 1 mol % PC loading.[46]

MeCN the yields drop drastically using each of the four PCs (Table 3, entries 2, 5, 8, and 11), while switching to DCM afforded product yields of 56%, 63%, 42%, and 48% for **DABNA-1**, ***t*DABNA**, **CzBN**, and **DtBuCzB**, respectively (Table 3, entries 3, 6, 9, and 12), all of which are higher than those reported using D-A TADF PCs. Product yields of 89%, 84%, 71%, and 39%, respectively, were obtained using the literature PCs **[Ru(bpy)$_3$](PF$_6$)$_2$**, ***fac*-Ir(ppy)$_3$**, **[Ir(ppy)$_2$(dtbbpy)](PF$_6$)**, and **4CzIPN**. The low yield for **4CzIPN** is surprising, as it should possess sufficient reducing power ($E_{ox}$* = −1.04 V vs. SCE[17]) to reduce TsCl ($E_{red}$ = −0.94 V vs. SCE).[46]

The photostability of ***t*DABNA** was investigated under the indicated reaction conditions (Figure 7B). As we had shown that this compound in solution is photostable in THF but not in DCM (Figure 7A), we wanted to determine whether there is a connection between the low yield in THF compared to DCM and the photostability of the PC. After irradiation in DCM and THF each, the absorption profile of ***t*DABNA** changed significantly, with the complete disappearance of the low-energy SRCT absorption band. This clearly shows that ***t*DABNA** is not stable under the reaction conditions regardless of the solvent used. In a comprehensive study, Bryden et al. have shown that the photostability of a wide range of PCs engaged in photoredox reactions is generally poor.[38]

### *Reductive quenching photoredox catalysis*

We next selected the pinacol coupling of benzaldehyde as a model reductive quenching reaction (Tables 4 and S9; Figures S52–S56), which involves PET from the sacrificial reductant, diisopropylethylamine (DIPEA), to the of PC* to form

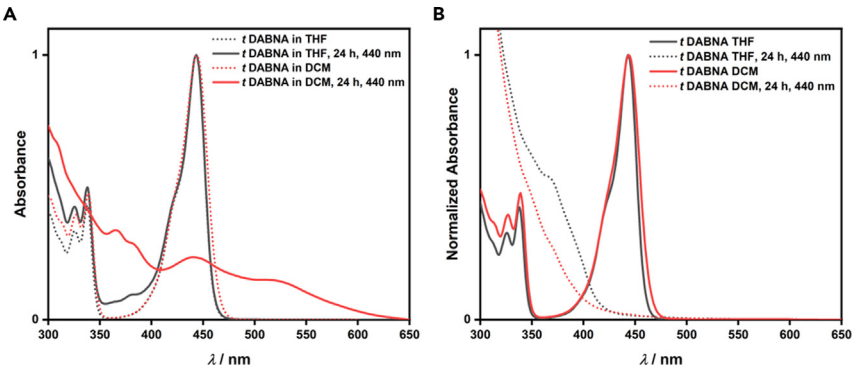


**Figure 7. Degradation study of *t*DABNA**

(A) ***t*DABNA** dissolved in THF and DCM and (B) ***t*DABNA** as the PC in the ATRA reaction. Reaction conditions were TsCl (0.25 mmol), styrene (0.50 mmol), and PC (3 mol %) in 1 mL solvent under inert conditions. Absorption before and after 24 h irradiation at 440 nm in THF and DCM is shown.

$PC^{-\bullet}$, which then reduces benzaldehyde with the assistance of $DIPEA^{+\bullet}$ (Figure S51).[50]

Gratifyingly, a yield of 70% was obtained using **CzBN** as the PC under a nitrogen atmosphere after 24 h (Table 4, entry 4). The yields were slightly lower using **DABNA-1**, ***t*DABNA**, and **DtBuCzB** at 64%, 61%, and 53%, respectively (Table 4, entries 2, 3, and 7). Decreasing the reaction time to 2 h resulted in a much lower yield of 36% (Table 4, entry 5). The literature-accepted mechanism involves a reductive quench of the PC* by DIPEA, which means that the $E_{red}$* of the PCs should be more positive than the oxidation potential of DIPEA ($E_{ox}$ = 0.86 V vs. SCE)[51] for the reaction to be exergonic. With $E_{red}$* = 0.96 V vs. SCE for **CzBN** in THF, **CzBN** is the only PC of the four in the study that possesses a more positive $E_{red}$* than the $E_{ox}$ of DIPEA. Control reactions under air led to no product formation using either **CzBN** or **DtBuCzB** (Table 4, entries 4 and 7 in parentheses); however, product yields of 29% and 35% were obtained using **DABNA-1** and ***t*DABNA**, respectively (Table 4, entries 2 and 3 in parentheses). One possible reason for this divergence in behavior would be the increased photostability of these two compounds in air under the reaction conditions compared to **CzBN** or **DtBuCzB**, as demonstrated in Figures 8A and 8B for two exemplar PCs, **DABNA-1** and **CzBN**. There are minimal changes in the absorption profiles of the reaction mixture with **DABNA-1** under both an inert and an aerated atmosphere after irradiation compared to the profiles before absorption, suggesting that **DABNA-1** is mostly photostable in these conditions. The slight change in the absorption spectra at higher energy is more pronounced under aerated conditions, which may explain the lower yields in air with this PC. The time-resolved PL decays of **DABNA-1** and **CzBN** under nitrogen in THF are similar, possessing a major prompt fluorescence component with lifetimes, $\tau_p$, of 10.4 and 7.6 ns, respectively, and a minor delayed fluorescence component with lifetimes, $\tau_d$, of 42.3 and 58.8 μs, respectively (Figure S54). Under air, the delayed fluorescence is completely quenched in both compounds, while the $\tau_p$ decreases modestly, 7.0 and 6.2 ns for **DABNA-1** and **CzBN**, respectively. Thus, there seems to be no correlation between competitive quenching of the excited state of these two PCs by $O_2$ and reaction yield, and it is at present unclear where there is such a divergence in reactivity between these two PCs under air other than the general photoinstability of **CzBN**. For **CzBN**, however, the absorption profiles under both inert and aerated atmospheres changed significantly after irradiation, implying that **CzBN** is unstable under these

**Table 4. Photocatalyzed pinacol coupling of benzaldehyde**

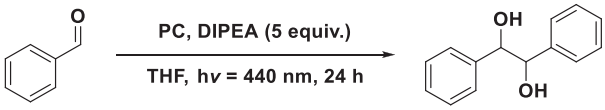


| Entry | Photocatalyst | $^1$H NMR yield (%) | $E_{red}$* (V) | $E_{red}$ (V) |
|---|---|---|---|---|
| 1 | no PC | 0 ± 0 | – | – |
| 2 | DABNA-1 (3 mol %) | 64 ± 2 (29 ± 0) | 0.52 | −2.24 |
| 3 | *t*DABNA (3 mol %) | 61 ± 4 (35 ± 4) | ND[a] | ND[a] |
| 4 | CzBN (3 mol %) | 70 ± 1 (0 ± 0) | 0.96 | −1.69 |
| 5 | CzBN (3 mol %), 2 h | 36 ± 0 | 0.96 | −1.69 |
| 6 | CzBN (3 mol %), dark | 0 ± 0 | 0.96 | −1.69 |
| 7 | DtBuCzB (3 mol %) | 53 ± 0 (0 ± 0) | 0.83 | −1.77 |
| 8 | *fac*-Ir(ppy)$_3$ (1 mol %) | 26 ± 2 (19 ± 1) | 0.31 | −2.19 |
| 9 | [Ru(bpy)$_3$](PF$_6$)$_2$ (1 mol %) | 3 ± 1 (0 ± 0) | 0.77 | −1.33 |
| 10 | 4CzIPN (1 mol %) | 71 ± 1 (73 ± 2); 68[b] | 1.35 | −1.21 |
| 11 | 4CzIPN (1 mol %), 2 h | 50 ± 0 | 1.35 | −1.21 |
| 12 | [Ir(ppy)$_2$(dtbbpy)](PF$_6$) (1 mol %) | 70 ± 4 (77 ± 2); 44[c] | 0.66 | −1.51 |
| 13 | [Ir(ppy)$_2$(dtbbpy)](PF$_6$) (1 mol %), 2 h | 69 ± 2 | 0.66 | −1.51 |

Benzaldehyde (0.2 mmol), DIPEA (1.0 mmol), and PC (3 mol %/1 mol %) in 1 mL solvent. Irradiated at 440 nm for 24 h at room temperature. Yield determined by $^1$H NMR spectroscopy using TMB as an internal standard. Reactions were carried out under an inert atmosphere, and yields in parentheses are under air.
[a]Reduction potential of **tDABNA** could not be determined in any solvent due to the too-limited solvent windows.
[b]Literature-reported yield after 2 h in DMF and $\lambda_{exc}$ = 390 nm.[19]
[c]Literature-reported yield after 15 h in MeCN and $\lambda_{exc}$ = 450 nm, 11 W compact fluorescent lamp (CFL).[50]

conditions. It is not evident why there is such a divergent photostability behavior between these two PCs nor how this is correlated to reaction yield.

The yields using the reference PCs ***fac*-Ir(ppy)$_3$**, **[Ru(bpy)$_3$](PF$_6$)$_2$**, **4CzIPN**, and **[Ir(ppy)$_2$(dtbbpy)](PF$_6$)** in THF under aerated conditions at 1 mol % loading, which is typically used in the literature, are 19%, 0%, 73%, and 77%, respectively (Table 4, entries 8, 9, 10, and 12 in parentheses). Of these PCs ($E_{red}$*[***fac*-Ir(ppy)$_3$**] = 0.31 V, $E_{red}$*[[Ru(bpy)$_3$](PF$_6$)$_2$] = 0.77 V, $E_{red}$*[**4CzIPN**] = 1.35 V, and $E_{red}$*[Ir(ppy)$_2$(dtbbpy)](PF$_6$)] = 0.66 V), **4CzIPN** has the strongest thermodynamically driving force for this reaction, which may explain the high product yield using this PC, but this argument is incongruent for **[Ir(ppy)$_2$(dtbbpy)](PF$_6$)**. Under an inert atmosphere, the yields only slightly improved to 26% and 3% using ***fac*-Ir(ppy)$_3$** and **[Ru(bpy)$_3$](PF$_6$)$_2$**, while when using **4CzIPN** and **[Ir(ppy)$_2$(dtbbpy)](PF$_6$)**, the yield decreased slightly to 71% and 70%, respectively (Table 4, entries 8, 9, 10, and 12). Of the three best-performing PCs, **CzBN**, **4CzIPN**, and **[Ir(ppy)$_2$(dtbbpy)](PF$_6$)**, **CzBN** has the highest molar absorptivity ($\varepsilon$ = 21, 6, and 2 × $10^3$ $M^{-1}$ $cm^{-1}$ for **CzBN**, **4CzIPN**, and **[Ir(ppy)$_2$(dtbbpy)]PF$_6$**, respectively) at the excitation wavelength (Figure S55). Thus, the reaction should proceed the fastest with this PC, assuming that the rate-determining step is the initial reductive quenching of the PC* with DIPEA. After 2 h, the product yields were 36%, 50%, and 69% using **CzBN**, **4CzIPN**, and **[Ir(ppy)$_2$(dtbbpy)](PF$_6$)**, respectively (Table 4, entries 5, 11, and 13), implying that the rate-determining step is not the initial PET to the PC*.

### *Energy transfer photocatalysis*

We next assessed if these four PCs could engage in Dexter PEnT photocatalysis, using the *E*/*Z* isomerization of alkenes as a model reaction. It is generally accepted that the $T_1$ energy of the PC should lie intermediate between those of the *E* and *Z*

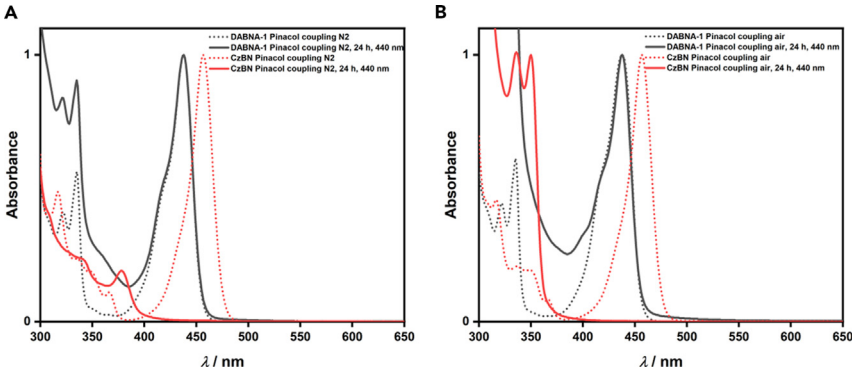


**Figure 8. Photodegradation study of DABNA-1 and CzBN**

Degradation study of the pinacol coupling reaction with **DABNA** and **CzBN** as the PC under (A) an inert atmosphere and (B) an aerated atmosphere. Reaction conditions were benzaldehyde (0.2 mmol), DIPEA (1.0 mmol), and PC (3 mol %) in THF (0.1 M). Absorption spectra before and after 24 h irradiation at 440 nm in THF are shown.

isomers to selectively photocatalyze the isomerization of the *E* isomer to the *Z* isomer (Figure S57). We assessed *E*-stilbene, di*iso*propyl fumarate, and cinnamyl acetate as Ss (Figures S58–S61; Table S10). The $E_T$ of *E*-stilbene and di*iso*propyl fumarate are 2.2[52] and 2.7 eV,[53] respectively, while the triplet energies of *Z*-stilbene and di*iso*propyl maleate are $E_T$ 2.5[52] and 3.1 eV,[53] respectively. *E*-methyl cinnamate, structurally similar to *E*-cinnamyl acetate, has a reported triplet energy of $E_T$ 2.38 V.[54]

**DABNA-1** performed the best with cinnamyl acetate as the S in THF, leading to an *E*/*Z* ratio of 24/76 after 24 h under an inert atmosphere (Table 5, entry 2). The yield did not effectively change under aerated conditions (*E*/*Z* ratio of 25/75; Table 5, entry 3), implying that Dexter energy transfer (DET) to the S outcompetes DET to $O_2$. Decreasing the reaction time to 2 h did not affect product yield (Table 5, entry 4). Using ***t*DABNA**, **CzBN**, and **DtBuCzB** as PCs resulted in *E*/*Z* ratios of 30/70, 20/80, and 22/78, respectively (Table 5, entries 5, 6, and 8), meaning that **CzBN** is the best PC of the four for this transformation. There seems to be a correlation between the reaction yield and the $\Delta E_{ST}$ of the PC, as **CzBN** has the smallest one at $\Delta E_{ST}$ 0.09 eV (cf. Table 1), implying that the triplet state of **CzBN** is more readily populated, as the ISC rate would be fastest for this compound. The *E*/*Z* ratios are comparable to those using **4CzIPN** and ***fac*-Ir(ppy)$_3$**, while **[Ru(bpy)$_3$](PF$_6$)$_2$** could not activate the photoisomerization of cinnamyl acetate (Table 5, entries 5–7).

## Conclusions

We have assessed the potential of four known boron-containing MR-TADF emitters as alternative PCs across a mechanistically diverse range of reactions. Certain conditions resulted in the PC not being photostable; however, this was not necessarily correlated with a reduction in product yield. Nonetheless, we found that there was variability in the PC that performed the best based on the model reactions surveyed. For instance, **DABNA-1** photosensitized the complete dehalogenation of methyl 4-chlorobenzoate, and ***t*DABNA** performed the best in an ATRA reaction with a 63% yield, while **4CzIPN** yielded only 39%; further, **CzBN** is the best PC in both the pinacol coupling (70% yield; **4CzIPN** yields 71%) and the energy transfer reaction (*E*/*Z* = 20/80 for cinnamyl acetate). This study demonstrates the value of these MR-TADF compounds as PCs to enable the activation of Ss with large reduction potentials while also providing versatility across a range of PET and PEnT reactions.

**Table 5. *E/Z* isomerization of cinnamyl acetate**

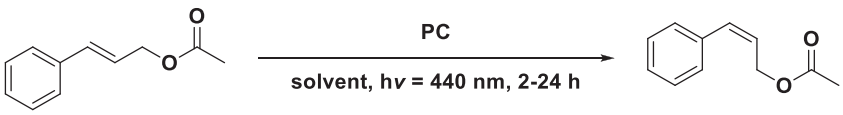


| Entry | Photocatalyst | *E/Z* ratio | $T_1$[a] (eV) |
|---|---|---|---|
| 1 | no PC | 100/0 ± 0 | – |
| 2 | DABNA-1 (inert atmosphere), 24 h | 24/76 ± 0 | 2.65 |
| 3 | DABNA-1 (aerated atmosphere), 24 h | 25/75 ± 0 | 2.65 |
| 4 | DABNA-1 (aerated atmosphere), 2 h | 25/75 ± 0 | 2.65 |
| 5 | *t*DABNA | 30/71 ± 1 | 2.64 |
| 6 | CzBN | 20/81 ± 1 | 2.57 |
| 7 | CzBN (dark) | 100/0 ± 0 | 2.57 |
| 8 | DtBuCzB | 22/78 ± 0 | 2.52 |
| 9 | 4CzIPN | 15/85 ± 0 | |
| 10 | *fac*-Ir(ppy)$_3$ | 23/78 ± 4 | 2.50 |
| 11 | [Ru(bpy)$_3$](PF$_6$)$_2$ | 100/0 ± 0 | 2.12 |

Cinnamyl acetate (0.2 mmol) and PC (3 mol %) in 1 mL solvent under aerated conditions unless otherwise noted. Irradiated at 440 nm for 2 h at room temperature. Ratio determined by $^1$H NMR spectroscopy of an average over two experiments.
[a]$T_1$ energy determined from the onset of the phosphorescence spectra at 77 K in 2-MeTHF glass.

This study reinforces the claim that MR-TADF compounds are competitive alternatives to common literature-known PCs.

## EXPERIMENTAL PROCEDURES

### Resource availability

#### *Lead contact*

Requests for further information and resources should be directed to and will be fulfilled by Prof. Eli Zysman-Colman (eli.zysman-colman@st-andrews.ac.uk).

#### *Materials availability*

This study did not generate new unique reagents.

#### *Data and code availability*

The research data supporting this publication can be accessed at https://doi.org/10.17630/3b81809a-fbbf-44f5-981a-30cde85eeef2.

### Dehalogenation of aryl halides

To an oven-dried vial was added methyl 4-chlorobenzoate (17.1 mg, 100 μmol, 1.0 equiv.) or methyl 4-bromobenzoate (21.5 mg, 100 μmol, 1.0 equiv.) or methyl 4-iodobenzoate (26.2 mg, 100 μmol, 1.0 equiv.), TMB (81.1 mg, 500 μmol, 5.0 equiv.), $Cs_2CO_3$ (65.2 mg, 200 μmol, 2.0 equiv.), and PC (5 mol %, 5.00 μmol). The vial was deoxygenated with vacuum/nitrogen cycles three times before dry MeCN (1 mL) was added. The reaction mixture was stirred and irradiated ($\lambda_{exc}$ = 440 nm) for 24 h. The crude reaction mixture was analyzed by $^1$H NMR spectroscopy.

### ATRA reaction

Styrene was deoxygenated via three freeze-pump-thaw cycles before being used in this reaction. To an oven-dried vial was added TsCl (47.7 mg, 250 μmol, 1.0 equiv.) and PC (3 mol %, 7.5 μmol) before being placed under $N_2$. Then dry solvent (1.0 mL) and styrene (52.1 mg, 500 μmol, 2.0 equiv.) were added. The reaction mixture was

stirred and irradiated ($\lambda_{exc}$ = 440 nm) for 24 h. The crude reaction mixture was analyzed by $^1$H NMR spectroscopy.

### Pinacol coupling

Benzaldehyde and DIPEA were each separately deoxygenated via freeze-pump-thaw (three cycles) before being used for the reaction carried out under $N_2$ atmosphere. To an oven-dried vial, PC (3 mol %, 6 μmol) was added and the vial placed under $N_2$. Then dry THF (2 mL) was added before benzaldehyde (21.2 mg, 200 μmol, 1.0 equiv.) and DIPEA (129 mg, 1.00 mmol, 5.0 equiv.) were added. The solution was stirred and irradiated ($\lambda_{exc}$ = 440 nm) for 24 h. The reaction mixture was analyzed via $^1$H NMR spectroscopy.

### *E*/*Z* isomerization

To an oven-dried vial was added the PC (1 mol %, 2 μmol) and (1) *E*-1,2-di-*p*-tolylethene (41.7 mg, 200 μmol, 1.0 equiv.), (2) di*iso*propyl fumarate (40.1 mg, 200 μmol, 1.0 equiv.), or (3) cinnamyl acetate (35.2 mg, 200 μmol, 1.0 equiv.) and solvent (1 mL). The solution was stirred at room temperature while being irradiated ($\lambda_{exc}$ = 440 nm) for 2 or 24 h. The reaction mixture was analyzed by $^1$H NMR spectroscopy.

## SUPPLEMENTAL INFORMATION

Supplemental information can be found online at https://doi.org/10.1016/j.checat.2024.101061.

## ACKNOWLEDGMENTS

We would like to thank the European Union H2020 research and innovation program for the funding under the Marie S. Curie Grant agreement (PhotoReAct, no. 956324). We thank Dr. John Marques Dos Santos for supplying **DtBuCzB** and Dr. Ettore Crovini for conducting initial steady-state emission studies. We thank Megan Bryden, Francis Millward, and Violaine Manet for providing samples of **4CzIPN**, *fac*-Ir(ppy)$_3$, [Ir(ppy)$_2$(dtbbpy)](PF$_6$), and [Ru(bpy)$_3$](PF$_6$)$_2$ and cyclic voltammetry studies of methyl 4-iodobenzoate. We thank Máire Griffin for conducting the **eosin Y** stability studies. We thank Prof. Daniele Leonori for discussions and for hosting L.H. for a secondment.

## AUTHOR CONTRIBUTIONS

E.Z.-C. conceived of and managed the project and supervised the work. L.H. carried out the synthesis of **DABNA-1**, ***t*DABNA**, **CzBN**, **DtBuCzB**, and **Ph-PTZ**; the photophysical and electrochemical analysis; and the photocatalysis reactions and the mechanistic studies. Both authors contributed to the manuscript writing and discussion.

## DECLARATION OF INTERESTS

The authors declare no competing interests.

Received: March 11, 2024
Revised: May 29, 2024
Accepted: June 21, 2024
Published: July 17, 2024

## REFERENCES

1. Shaw, M.H., Twilton, J., and MacMillan, D.W.C. (2016). Photoredox Catalysis in Organic Chemistry. J. Org. Chem. *81*, 6898–6926. https://doi.org/10.1021/acs.joc.6b01449.

2. Schultz, D.M., and Yoon, T.P. (2014). Solar Synthesis: Prospects in Visible Light Photocatalysis. Science *343*, 1239176. https://doi.org/10.1126/science.1239176.

3. Bryden, M.A., and Zysman-Colman, E. (2021). Organic thermally activated delayed fluorescence (TADF) compounds used in photocatalysis. Chem. Soc. Rev. *50*, 7587–7680. https://doi.org/10.1039/d1cs00198a.

4. Strieth-Kalthoff, F., James, M.J., Teders, M., Pitzer, L., and Glorius, F. (2018). Energy transfer catalysis mediated by visible light: principles, applications, directions. Chem. Soc. Rev. *47*, 7190–7202. https://doi.org/10.1039/c8cs00054a.

5. Ravelli, D., Fagnoni, M., and Albini, A. (2013). Photoorganocatalysis. What for? Chem. Soc. Rev. *42*, 97–113. https://doi.org/10.1039/C2CS35250H.

6. Romero, N.A., and Nicewicz, D.A. (2016). Organic Photoredox Catalysis. Chem. Rev. *116*, 10075–10166. https://doi.org/10.1021/acs.chemrev.6b00057.

7. Zeitler, K. (2018). Metal-Free Photo(redox) Catalysis. In Visible Light Photocatalysis in Organic Chemistry, C.R.J. Stephenson, T.P. Yoon, and D.W. MacMillan, eds. (Wiley-VCH), pp. 159–232.

8. Nicewicz, D.A., and Nguyen, T.M. (2014). Recent Applications of Organic Dyes as Photoredox Catalysts in Organic Synthesis. ACS Catal. *4*, 355–360. https://doi.org/10.1021/cs400956a.

9. Yan, D.-M., Chen, J.-R., and Xiao, W.-J. (2019). New Roles for Photoexcited Eosin Y in Photochemical Reactions. Angew. Chem. Int. Ed. *58*, 378–380. https://doi.org/10.1002/anie.201811102.

10. Sharma, S., and Sharma, A. (2019). Recent advances in photocatalytic manipulations of Rose Bengal in organic synthesis. Org. Biomol. Chem. *17*, 4384–4405. https://doi.org/10.1039/C9OB00092E.

11. Srivastava, A., Singh, P.K., Ali, A., Singh, P.P., and Srivastava, V. (2020). Recent applications of Rose Bengal catalysis in N-heterocycles: a short review. RSC Adv. *10*, 39495–39508. https://doi.org/10.1039/D0RA07400D.

12. Choi, W.O., Jung, Y.J., Kim, M., Kim, H., Li, J., Ko, H., Lee, H.-I., Lee, H.J., and Lee, J.K. (2023). Substituent Effects of Fluorescein on Photoredox Initiating Performance under Visible Light. ACS Omega *8*, 40277–40286. https://doi.org/10.1021/acsomega.3c04324.

13. Sun, W., Chen, H., Wang, K., Wang, X., Lei, M., Liu, C., and Zhong, Q. (2021). Synthesis of benzothiazoles using fluorescein as an efficient photocatalyst under visible light. Mol. Catal. *510*, 111693. https://doi.org/10.1016/j.mcat.2021.111693.

14. Joshi-Pangu, A., Lévesque, F., Roth, H.G., Oliver, S.F., Campeau, L.C., Nicewicz, D., and DiRocco, D.A. (2016). Acridinium-Based Photocatalysts: A Sustainable Option in Photoredox Catalysis. J. Org. Chem. *81*, 7244–7249. https://doi.org/10.1021/acs.joc.6b01240.

15. Tlili, A., and Lakhdar, S. (2021). Acridinium Salts and Cyanoarenes as Powerful Photocatalysts: Opportunities in Organic Synthesis. Angew. Chem. Int. Ed. *60*, 19526–19549. https://doi.org/10.1002/anie.202102262.

16. Wong, M.Y., and Zysman-Colman, E. (2017). Purely Organic Thermally Activated Delayed Fluorescence Materials for Organic Light-Emitting Diodes. Adv. Mater. *29*, 1605444. https://doi.org/10.1002/adma.201605444.

17. Luo, J., and Zhang, J. (2016). Donor–Acceptor Fluorophores for Visible-Light-Promoted Organic Synthesis: Photoredox/Ni Dual Catalytic C(sp3)–C(sp2) Cross-Coupling. ACS Catal. *6*, 873–877. https://doi.org/10.1021/acscatal.5b02204.

18. Speckmeier, E., Fischer, T.G., and Zeitler, K. (2018). A Toolbox Approach To Construct Broadly Applicable Metal-Free Catalysts for Photoredox Chemistry: Deliberate Tuning of Redox Potentials and Importance of Halogens in Donor-Acceptor Cyanoarenes. J. Am. Chem. Soc. *140*, 15353–15365. https://doi.org/10.1021/jacs.8b08933.

19. Bryden, M.A., Millward, F., Matulaitis, T., Chen, D., Villa, M., Fermi, A., Cetin, S., Ceroni, P., and Zysman-Colman, E. (2023). Moving Beyond Cyanoarene Thermally Activated Delayed Fluorescence Compounds as Photocatalysts: An Assessment of the Performance of a Pyrimidyl Sulfone Photocatalyst in Comparison to 4CzIPN. J. Org. Chem. *88*, 6364–6373. https://doi.org/10.1021/acs.joc.2c01137.

20. Bouzrati-Zerelli, M., Guillaume, N., Goubard, F., Bui, T.-T., Villotte, S., Dietlin, C., Morlet-Savary, F., Gigmes, D., Fouassier, J.P., Dumur, F., and Lalevée, J. (2018). A novel class of photoinitiators with a thermally activated delayed fluorescence (TADF) property. New J. Chem. *42*, 8261–8270. https://doi.org/10.1039/c7nj04394e.

21. Hojo, R., Bergmann, K., Elgadi, S.A., Mayder, D.M., Emmanuel, M.A., Oderinde, M.S., and Hudson, Z.M. (2023). Imidazophenothiazine-Based Thermally Activated Delayed Fluorescence Materials with Ultra-Long-Lived Excited States for Energy Transfer Photocatalysis. J. Am. Chem. Soc. *145*, 18366–18381. https://doi.org/10.1021/jacs.3c04132.

22. Sauvé, E.R., Mayder, D.M., Kamal, S., Oderinde, M.S., and Hudson, Z.M. (2022). An imidazoacridine-based TADF material as an effective organic photosensitizer for visible-light-promoted [2 + 2] cycloaddition. Chem. Sci. *13*, 2296–2302. https://doi.org/10.1039/D1SC05098B.

23. Prentice, C., Morrison, J., Smith, A.D., and Zysman-Colman, E. (2023). Multi-Resonant Thermally Activated Delayed Fluorescent (MR-TADF) Compounds as Photocatalysts. Chem. Eur J. *29*, e202202998. https://doi.org/10.1002/chem.202202998.

24. Madayanad Suresh, S., Hall, D., Beljonne, D., Olivier, Y., and Zysman-Colman, E. (2020). Multiresonant Thermally Activated Delayed Fluorescence Emitters Based on Heteroatom-Doped Nanographenes: Recent Advances and Prospects for Organic Light-Emitting Diodes. Adv. Funct. Mater. *30*, 1908677. https://doi.org/10.1002/adfm.201908677.

25. Arias-Rotondo, D.M., and McCusker, J.K. (2016). The photophysics of photoredox catalysis: a roadmap for catalyst design. Chem. Soc. Rev. *45*, 5803–5820. https://doi.org/10.1039/C6CS00526H.

26. Noël, T., and Zysman-Colman, E. (2022). The promise and pitfalls of photocatalysis for organic synthesis. Chem Catal. *2*, 468–476. https://doi.org/10.1016/j.checat.2021.12.015.

27. Poelma, S.O., Burnett, G.L., Discekici, E.H., Mattson, K.M., Treat, N.J., Luo, Y., Hudson, Z.M., Shankel, S.L., Clark, P.G., Kramer, J.W., et al. (2016). Chemoselective Radical Dehalogenation and C–C Bond Formation on Aryl Halide Substrates Using Organic Photoredox Catalysts. J. Org. Chem. *81*, 7155–7160. https://doi.org/10.1021/acs.joc.6b01034.

28. Theriot, J.C., Lim, C.-H., Yang, H., Ryan, M.D., Musgrave, C.B., and Miyake, G.M. (2016). Organocatalyzed atom transfer radical polymerization driven by visible light. Science *352*, 1082–1086. https://doi.org/10.1126/science.aaf3935.

29. Discekici, E.H., Treat, N.J., Poelma, S.O., Mattson, K.M., Hudson, Z.M., Luo, Y., Hawker, C.J., and Read de Alaniz, J. (2015). A highly reducing metal-free photoredox catalyst: design and application in radical dehalogenations. Chem. Commun. *51*, 11705–11708. https://doi.org/10.1039/c5cc04677g.

30. Hatakeyama, T., Shiren, K., Nakajima, K., Nomura, S., Nakatsuka, S., Kinoshita, K., Ni, J., Ono, Y., and Ikuta, T. (2016). Ultrapure Blue Thermally Activated Delayed Fluorescence Molecules: Efficient HOMO-LUMO Separation by the Multiple Resonance Effect. Adv. Mater. *28*, 2777–2781. https://doi.org/10.1002/adma.201505491.

31. Han, S.H., Jeong, J.H., Yoo, J.W., and Lee, J.Y. (2019). Ideal blue thermally activated delayed fluorescence emission assisted by a thermally activated delayed fluorescence assistant dopant through a fast reverse intersystem crossing mediated cascade energy transfer process. J. Mater. Chem. C *7*, 3082–3089. https://doi.org/10.1039/c8tc06575f.

32. Xu, S., Yang, Q., Zhang, Y., Li, H., Xue, Q., Xie, G., Gu, M., Jin, J., Huang, L., and Chen, R. (2021). Solution-processed multi-resonance organic light-emitting diodes with high efficiency and narrowband emission. Chin. Chem. Lett. *32*, 1372–1376. https://doi.org/10.1016/j.cclet.2020.10.022.

33. Xu, Y., Cheng, Z., Li, Z., Liang, B., Wang, J., Wei, J., Zhang, Z., and Wang, Y. (2020). Molecular-Structure and Device-Configuration Optimizations toward Highly Efficient Green Electroluminescence with Narrowband Emission and High Color Purity. Adv. Opt. Mater. *8*, 1902142. https://doi.org/10.1002/adom.201902142.

34. Koike, T., and Akita, M. (2014). Visible-light radical reaction designed by Ru- and Ir-based photoredox catalysis. Inorg. Chem. Front. *1*, 562–576. https://doi.org/10.1039/C4QI00053F.

35. Flamigni, L., Barbieri, A., Sabatini, C., Ventura, B., and Barigelletti, F. (2007). Photochemistry and Photophysics of Coordination Compounds: Iridium. In Photochemistry and Photophysics of Coordination Compounds II, V. Balzani and S. Campagna, eds. (Springer Berlin Heidelberg), pp. 143–203. https://doi.org/10.1007/128_2007_131.

36. Hall, D., Suresh, S.M., dos Santos, P.L., Duda, E., Bagnich, S., Pershin, A., Rajamalli, P., Cordes, D.B., Slawin, A.M.Z., Beljonne, D., et al. (2020). Improving Processability and Efficiency of Resonant TADF Emitters: A Design Strategy. Adv. Opt. Mater. *8*, 1901627. https://doi.org/10.1002/adom.201901627.

37. Lowry, M.S., Goldsmith, J.I., Slinker, J.D., Rohl, R., Pascal, R.A., Malliaras, G.G., and Bernhard, S. (2005). Single-Layer Electroluminescent Devices and Photoinduced Hydrogen

Production from an Ionic Iridium(III) Complex. Chem. Mater. *17*, 5712–5719. https://doi.org/10.1021/cm051312+.

38. Bryden, M.A., Millward, F., Lee, O.S., Cork, L., Gather, M.C., Steffen, A., and Zysman-Colman, E. (2024). Lessons learnt in photocatalysis – the influence of solvent polarity and the photostability of the photocatalyst. Chem. Sci. *15*, 3741–3757. https://doi.org/10.1039/D3SC06499A.

39. Donabauer, K., Maity, M., Berger, A.L., Huff, G.S., Crespi, S., and König, B. (2019). Photocatalytic carbanion generation – benzylation of aliphatic aldehydes to secondary alcohols. Chem. Sci. *10*, 5162–5166. https://doi.org/10.1039/C9SC01356C.

40. Grotjahn, S., and König, B. (2021). Photosubstitution in Dicyanobenzene-based Photocatalysts. Org. Lett. *23*, 3146–3150. https://doi.org/10.1021/acs.orglett.1c00836.

41. Alvarez-Martin, A., Trashin, S., Cuykx, M., Covaci, A., De Wael, K., and Janssens, K. (2017). Photodegradation mechanisms and kinetics of Eosin-Y in oxic and anoxic conditions. Dyes Pigments *145*, 376–384. https://doi.org/10.1016/j.dyepig.2017.06.031.

42. Bryden, M.A., Crovini, E., Comerford, T., Studer, A., and Zysman-Colman, E. (2024). Organic Donor-Acceptor Thermally Activated Delayed Fluorescence Photocatalysts in the Photoinduced Dehalogenation of Aryl Halides. Angewandte Chemie International Edition *n/a*. Angew. Chem., Int. Ed. Engl. *63*, e202405081. https://doi.org/10.1002/anie.202405081.

43. Constantin, T., Zanini, M., Regni, A., Sheikh, N.S., Juliá, F., and Leonori, D. (2020). Aminoalkyl radicals as halogen-atom transfer agents for activation of alkyl and aryl halides. Science *367*, 1021–1026. https://doi.org/10.1126/science.aba2419.

44. Bock, C.R., Connor, J.A., Gutierrez, A.R., Meyer, T.J., Whitten, D.G., Sullivan, B.P., and Nagle, J.K. (1979). Estimation of excited-state redox potentials by electron-transfer quenching. Application of electron-transfer theory to excited-state redox processes. J. Am. Chem. Soc. *101*, 4815–4824. https://doi.org/10.1021/ja00511a007.

45. Pintauer, T., and Matyjaszewski, K. (2008). Atom transfer radical addition and polymerization reactions catalyzed by ppm amounts of copper complexes. Chem. Soc. Rev. *37*, 1087–1097. https://doi.org/10.1039/B714578K.

46. Hossain, A., Engl, S., Lutsker, E., and Reiser, O. (2019). Visible-Light-Mediated Regioselective Chlorosulfonylation of Alkenes and Alkynes: Introducing the Cu(II) Complex [Cu(dap)Cl2] to Photochemical ATRA Reactions. ACS Catal. *9*, 1103–1109. https://doi.org/10.1021/acscatal.8b04188.

47. Engl, S., and Reiser, O. (2022). Copper-photocatalyzed ATRA reactions: concepts, applications, and opportunities. Chem. Soc. Rev. *51*, 5287–5299. https://doi.org/10.1039/D2CS00303A.

48. Singh, V.K., Yu, C., Badgujar, S., Kim, Y., Kwon, Y., Kim, D., Lee, J., Akhter, T., Thangavel, G., Park, L.S., et al. (2018). Highly efficient organic photocatalysts discovered via a computer-aided-design strategy for visible-light-driven atom transfer radical polymerization. Nat. Catal. *1*, 794–804. https://doi.org/10.1038/s41929-018-0156-8.

49. Polgar, A.M., Huang, S.H., and Hudson, Z.M. (2022). Donor modification of thermally activated delayed fluorescence photosensitizers for organocatalyzed atom transfer radical polymerization. Polym. Chem. *13*, 3892–3903. https://doi.org/10.1039/D2PY00470D.

50. Nakajima, M., Fava, E., Loescher, S., Jiang, Z., and Rueping, M. (2015). Photoredox-Catalyzed Reductive Coupling of Aldehydes, Ketones, and Imines with Visible Light. Angew. Chem. Int. Ed. *54*, 8828–8832. https://doi.org/10.1002/anie.201501556.

51. Goliszewska, K., Rybicka-Jasińska, K., Clark, J.A., Vullev, V.I., and Gryko, D. (2020). Photoredox Catalysis: The Reaction Mechanism Can Adjust to Electronic Properties of a Catalyst. ACS Catal. *10*, 5920–5927. https://doi.org/10.1021/acscatal.0c00200.

52. Herkstroeter, W.G., and McClure, D.S. (1968). The lowest triplet state of stilbene. J. Am. Chem. Soc. *90*, 4522–4527.

53. Lu, J., Pattengale, B., Liu, Q., Yang, S., Shi, W., Li, S., Huang, J., and Zhang, J. (2018). Donor-Acceptor Fluorophores for Energy-Transfer-Mediated Photocatalysis. J. Am. Chem. Soc. *140*, 13719–13725. https://doi.org/10.1021/jacs.8b07271.

54. Schmid, L., Kerzig, C., Prescimone, A., and Wenger, O.S. (2021). Photostable Ruthenium(II) Isocyanoborato Luminophores and Their Use in Energy Transfer and Photoredox Catalysis. JACS Au *1*, 819–832. https://doi.org/10.1021/jacsau.1c00137.

55. Tsuchiya, Y., Diesing, S., Bencheikh, F., Wada, Y., dos Santos, P.L., Kaji, H., Zysman-Colman, E., Samuel, I.D.W., and Adachi, C. (2021). Exact Solution of Kinetic Analysis for Thermally Activated Delayed Fluorescence Materials. J. Phys. Chem. A *125*, 8074–8089. https://doi.org/10.1021/acs.jpca.1c04056.

56. Treat, N.J., Sprafke, H., Kramer, J.W., Clark, P.G., Barton, B.E., Read de Alaniz, J., Fors, B.P., and Hawker, C.J. (2014). Metal-free atom transfer radical polymerization. J. Am. Chem. Soc. *136*, 16096–16101. https://doi.org/10.1021/ja510389m.

57. Sajoto, T., Djurovich, P.I., Tamayo, A.B., Oxgaard, J., Goddard, W.A., III, and Thompson, M.E. (2009). Temperature Dependence of Blue Phosphorescent Cyclometalated Ir(III) Complexes. J. Am. Chem. Soc. *131*, 9813–9822. https://doi.org/10.1021/ja903317w.

58. Chen, D.-F., Chrisman, C.H., and Miyake, G.M. (2020). Bromine Radical Catalysis by Energy Transfer Photosensitization. ACS Catal. *10*, 2609–2614. https://doi.org/10.1021/acscatal.0c00281.

59. Ladouceur, S., Fortin, D., and Zysman-Colman, E. (2011). Enhanced Luminescent Iridium(III) Complexes Bearing Aryltriazole Cyclometallated Ligands. Inorg. Chem. *50*, 11514–11526. https://doi.org/10.1021/ic2014013.

60. Juris, A., Balzani, V., Belser, P., and von Zelewsky, A. (1981). Characterization of the Excited State Properties of Some New Photosensitizers of the Ruthenium (Polypyridine) Family. Helv. Chim. Acta *64*, 2175–2182. https://doi.org/10.1002/hlca.19810640723.

61. Kalyanasundaram, K. (1982). Photophysics, photochemistry and solar energy conversion with tris(bipyridyl)ruthenium(II) and its analogues. Coord. Chem. Rev. *46*, 159–244. https://doi.org/10.1016/0010-8545(82)85003-0.

62. Juris, A., Balzani, V., Barigelletti, F., Campagna, S., Belser, P., and von Zelewsky, A. (1988). Ru(II) polypyridine complexes: photophysics, photochemistry, eletrochemistry, and chemiluminescence. Coord. Chem. Rev. *84*, 85–277. https://doi.org/10.1016/0010-8545(88)80032-8.